



pubs.acs.org/JPCC Article

# A Model for the Concentration Admittance of a Polymer Electrolyte Fuel Cell

Ying Sun,\* Thomas Kadyk, Andrei Kulikovsky,\* and Michael Eikerling



Cite This: J. Phys. Chem. C 2022, 126, 14075-14081

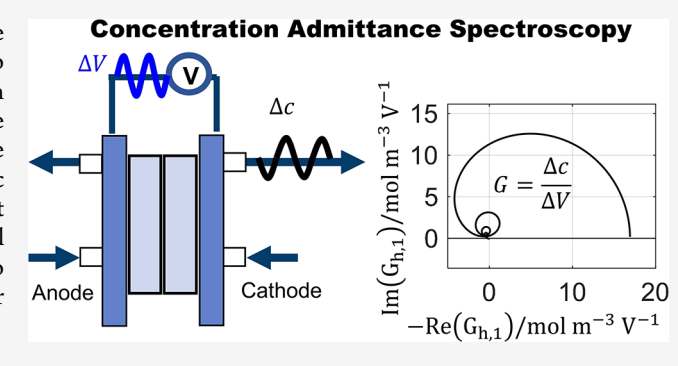


**ACCESS** I

Metrics & More

Article Recommendations

ABSTRACT: A dynamic model for the concentration admittance of a polymer electrolyte fuel cell is presented. The model takes into account oxygen transport in the cathode channel, the gas diffusion layer, and the cathode catalyst layer. An analytical solution for the concentration admittance is derived. We observe that the admittance at the air channel outlet is not affected by faradaic reactions, and it contains information on the oxygen transport coefficients in the cell. The admittance measured at the air channel outlet can be fitted using the formula obtained in this work to extract the oxygen transport coefficients. Practical methods for measuring the concentration admittance are proposed.



# **■ INTRODUCTION**

Polymer electrolyte fuel cells (PEFCs) are a key technology to enable a sustainable future energy ecosystem with a much reduced carbon footprint. Further efforts to markedly improve the performance of PEFCs hinge on diagnostic capabilities to separate and quantify voltage losses due to electrochemical reactions and mass transport processes. In this realm, electrochemical impedance spectroscopy (EIS) is a mature approach that is extensively used for the nondestructive and inoperando assessment of the performance (state of health) of cells in a PEFC stack.

The rate (or current density) of the oxygen reduction reaction (ORR) depends on the oxygen concentration, c, as well as on the electrode potential, E. Therefore, a small-amplitude periodic perturbation of either c or E causes a transient response of the fuel cell current density. In analogy to the EIS response, an oxygen concentration impedance,  $\zeta = \delta E/\delta c$ , can be defined that allows probing the oxygen transport processes on the cathode side of the PEFC. Here  $\delta E$  and  $\delta c$  are the small-amplitude harmonic perturbations of electrode potential and oxygen concentration.

However, oxygen concentration can either be the input signal or the measured response. The former approach has been investigated both experimentally and theoretically in the past decade. In 2009, Niroumand et al. generated a concentration/pressure (C/P) impedance by perturbing the cathode outlet pressure at 0.14 Hz and proposed the concept of C/P impedance spectroscopy to analyze liquid water transport in the cell. From then on, experimental measurements of C/P impedance spectroscopy of PEFCs have been carried out consecutively. Engebretsen et al. perturbed the

cathode outlet pressure using a loudspeaker and measured the voltage response from 10 mHz to 100 Hz. The pressure impedance has been found to be sensitive to relative humidity. Zhang et al.<sup>3,4</sup> and Shirsath et al.<sup>5</sup> used a back-pressure controller to generate oscillations in cathode outlet pressure and investigated the effect of operating conditions, such as voltage load, oxygen concentration, or oxygen stoichiometry, on pressure impedance.

The aforementioned studies are limited to qualitative parametric studies due to the lack of models for extracting oxygen transport properties. Schiffer et al. developed a model for pressure impedance spectroscopy and reported a good agreement with experiments at a current density lower than 0.4 A/cm<sup>2</sup>; they attributed the experimentally observed maximum in the amplitude of pressure impedance to a resonance in the oxygen partial pressure. Sorrentino et al.  $^{7-9}$  measured C/Pspectra of a PEFC by applying perturbation in oxygen concentration at the cathode inlet and developed numerical models for the C/P impedance. Kulikovsky  $^{10}$  developed an analytical model for the C/P impedance under the assumption of an infinite air flow stoichiometry and a large voltage loss incurred by oxygen transport in the catalyst layer. Species Frequency Response Analysis (sFRA), which applies current perturbation and measures the response of the flux of volatile

Received: June 15, 2022 Revised: July 28, 2022 Published: August 16, 2022





species via differential electrochemical mass spectrometry, has been proposed and demonstrated for the electrochemical methanol oxidation reaction on a porous Pt/Ru electrode by Kubannek et al. While sFRA uses a current perturbation and is applied to analyze methanol oxidation in a cyclone flow cell, it is demonstrated that the method is practically applicable and reaction and transport parameters can be deconvoluted with a proper model. A sensitivity analysis confirms that sFRA is sensitive to transport parameters that are not accessible by EIS.

Measuring the oxygen concentration response,  $\delta c$ , while perturbing the system with a small-amplitude modulation in electrode potential,  $\delta E$ , or cell current density,  $\delta j$ , has not been exploited so far. This work aims to demonstrate the potential of concentration admittance spectroscopy (CAS), which is based on measuring the ratio  $\delta c/\delta E$ . CAS is chosen due to its finite amplitude, while the amplitude of the concentration impedance diverges (see below).

In this work, we develop a quasi-2D model for the PEFC cathode side concentration admittance, which accounts for oxygen transport in the cathode catalyst layer (CCL), gas diffusion layer (GDL), and flow field (FF). An analytical expression for the concentration admittance is derived. Concentration admittance spectroscopy thus realized does not require perturbation of external pressure or concentration. Instead, it is based on measuring  $\delta c$  at the cathode channel outlet during a standard EIS measurement. We suggest and discuss methods for measuring  $\delta c$  at the cathode outlet.

#### MODEL

The model takes into account oxygen transport in the CCL, GDL and channel. Quasi-2D modeling, as depicted in Figure 1,

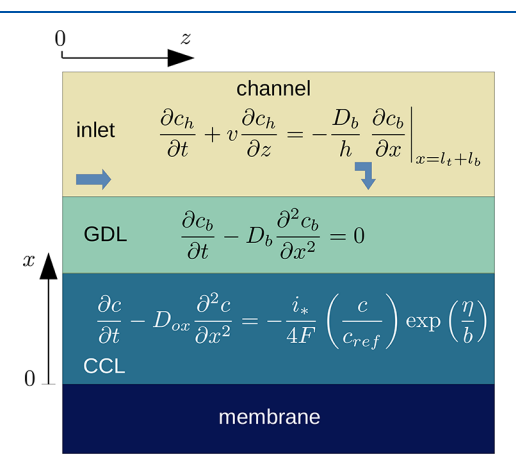


**Figure 1.** Schematic of the cathode side of a PEFC with a straight flow field channel, the gas diffusion layer, and the cathode catalyst layer. Shown are the oxygen mass transport equations in each transport element.

links oxygen transport in through-plane direction (along the x-axis) with transport along the air channel (along the z-axis). The model employs the following assumptions:

- High electronic conductivity of the cell components exists, meaning that the ORR overpotential  $\eta$  is nearly independent of the location along the z-axis.
- Proton transport in the CCL is fast, meaning that the static  $\eta^0$  and perturbed  $\eta^1$  shapes of the ORR overpotential are nearly independent of x.

The first assumption usually holds for typical PEM fuel cells. The second assumption limits the cell current density  $J: J \ll \sigma_t b/l_v$  where  $l_t$  is the CCL thickness,  $\sigma_t$  is the CCL proton conductivity, and b is the ORR Tafel slope.

To simplify calculations, dimensionless variables are introduced according to

$$\tilde{x} = \frac{x}{l_t}, \quad \tilde{z} = \frac{z}{L}, \quad \tilde{l}_b = \frac{l_b}{l_t}, \quad \tilde{t} = \frac{ti_*}{4Fc_h^{in}}, \quad \tilde{c} = \frac{c}{c_h^{in}},$$

$$\tilde{\eta} = \frac{\eta}{b}, \quad \tilde{j} = \frac{j}{l_t i_*}, \quad \tilde{\omega} = \frac{4F\omega c_h^{in}}{i_*}, \quad \tilde{D} = \frac{4FDc_h^{in}}{l_t^2 i_*},$$

$$\tilde{v} = \frac{4Fvc_h^{in}}{i_*L}, \quad \tilde{h} = \frac{h}{l_t}$$
(1)

where the tilde sign marks the dimensionless variables, x is the coordinate through the cell, z is the coordinate along the channel,  $l_b$  is the GDL thickness, L is the length of the straight channel, h is the channel depth, t is time,  $i_*$  is the ORR volumetric exchange current density, j is the local proton current density in the CCL, F is the Faraday constant,  $c_h^{in}$  is the reference (inlet) oxygen concentration, c is the oxygen concentration, c is the oxygen convention, c is the angular frequency, c is the oxygen diffusivity, and c is the air flow velocity in the channel.

**Through-Plane Direction.** Basic Equations and Static Solutions. Oxygen transport in CCL and GDL is described by eq 2 and eq 3, respectively:

$$\frac{\partial c}{\partial t} - D_{ox} \frac{\partial^2 c}{\partial x^2} = -\frac{i_*}{4F} \left(\frac{c}{c_h^{in}}\right) \exp\left(\frac{\eta}{b}\right)$$
(2)

$$\frac{\partial c_b}{\partial t} - D_b \frac{\partial^2 c_b}{\partial x^2} = 0 \tag{3}$$

Here c and  $c_b$  are the oxygen concentrations in CCL and GDL, and  $D_{ox}$  and  $D_b$  are the oxygen diffusivity of CCL and GDL, respectively. The right side of eq 2 describes the rate of oxygen consumption in a four-electron ORR.

With dimensionless variables, eqs 2 and 3 transform to

$$\frac{\partial \tilde{c}}{\partial \tilde{t}} - \tilde{D}_{ox} \frac{\partial^2 \tilde{c}}{\partial \tilde{x}^2} = -\tilde{c} e^{\tilde{\eta}}$$
(4)

$$\frac{\partial \tilde{c}_b}{\partial \tilde{t}} - \tilde{D}_b \frac{\partial^2 \tilde{c}_b}{\partial \tilde{x}^2} = 0 \tag{5}$$

The static oxygen concentration curve in the CCL and GDL is determined by eq 6 and eq 7:

$$\tilde{D}_{ox} \frac{\partial^2 \tilde{c}^0}{\partial \tilde{x}^2} = \tilde{c}^0 e^{\tilde{\eta}^0}, \quad \left. \frac{\partial \tilde{c}^0}{\partial \tilde{x}} \right|_{\tilde{x}=0} = 0, \quad \tilde{c}^0(1) = \tilde{c}_b^0(1) \equiv \tilde{c}_1^0$$
(6)

$$\tilde{D}_{b} \frac{\partial^{2} \tilde{c}_{b}^{0}}{\partial \tilde{x}^{2}} = 0, \quad \tilde{D}_{b} \frac{\partial \tilde{c}_{b}^{0}}{\partial \tilde{x}} \bigg|_{\tilde{x}=1+} = \tilde{D}_{ox} \frac{\partial \tilde{c}^{0}}{\partial \tilde{x}} \bigg|_{\tilde{x}=1-},$$

$$\tilde{c}_{b}^{0} (1 + \tilde{l}_{b}) = \tilde{c}_{b}^{0} \tag{7}$$

Here,  $\tilde{c}^0$  and  $\tilde{c}^0_b$  are the normalized static oxygen concentrations in the CCL and GDL, and  $\tilde{c}^0_1$  and  $\tilde{c}^0_h$  are the normalized static oxygen concentrations at the CCL/GDL interface and at the GDL/channel interface, respectively. The left boundary condition in eq 6 refers to the impermeable nature of the

membrane for oxygen, resulting in zero flux, while the right boundary condition describes continuity of the oxygen concentration at the CCL/GDL interface. The left boundary condition in eq 7 refers to continuity of the oxygen flux at the CCL/GDL interface, and the right boundary condition stands for a fixed oxygen concentration at the GDL/channel interface.

The solutions for  $\tilde{c}^0$  and  $\tilde{c}^0_b$  are

$$\tilde{c}^{0}(\tilde{x}) = \frac{\tilde{c}_{1}^{0} \cosh(\phi_{0}\tilde{x})}{\cosh(\phi_{0})} \tag{8}$$

$$\tilde{c}_b^{\,0}(\tilde{x}) = \frac{\tilde{D}_{ox}\tilde{c}_1^{\,0}\phi_0\,\tanh(\phi_0)}{\tilde{D}_b}(\tilde{x}-1-\tilde{l}_b) + \tilde{c}_h^{\,0} \tag{9}$$

where  $\phi_0$  is given as

$$\phi_0 = \sqrt{\frac{e^{\tilde{\eta}^0}}{\tilde{D}_{ox}}} \tag{10}$$

Setting in eq 9  $\tilde{x} = 1$  and taking into account the continuity of the oxygen concentration  $\tilde{c}_b^0(1) = \tilde{c}_1^0$ , we get an equation for  $\tilde{c}_0^0$ .

$$\tilde{c}_1^0 = \frac{\tilde{c}_h^0}{1 + \frac{\tilde{D}_{ox}\phi_0 \tanh(\phi_0)\tilde{l}_b}{\tilde{D}_b}}$$
(11)

The static oxygen concentration in the channel,  $\tilde{c}_h^0$  under small current density can be approximated by eq 12<sup>12</sup>,

$$\tilde{c}_h^0 = \left(1 - \frac{1}{\lambda}\right)^{\tilde{z}} \tag{12}$$

where  $\lambda$  is the stoichiometry of air flow,

$$\lambda = \frac{4Fhvc_h^{in}}{JL} \tag{13}$$

Substituting eq 12 into eq 11, we obtain the dependence of  $\tilde{c}_1^0$  on  $\tilde{z}_2$ ,

$$\tilde{c}_{1}^{0}(\tilde{z}) = \frac{1}{1 + \frac{\tilde{D}_{0x}\phi_{0}\tanh(\phi_{0})\tilde{I}_{b}}{\tilde{D}_{b}}} \left(1 - \frac{1}{\lambda}\right)^{\tilde{z}}$$
(14)

Zeta-Admittance. Calculations in this section have been reported in ref 10. For completeness, we repeat the derivation of the through-plane zeta-admittance, which is necessary for understanding further calculations. Linearization and Fourier-transformation of eq 4 and eq 5 leads to a system of linear equations for the small perturbation amplitudes  $\tilde{c}^1$ ,  $\tilde{c}^1_b$ ,  $\tilde{c}^1_b$ , and  $\tilde{\eta}^1$  in ω-space, 13

$$\begin{split} \tilde{D}_{ox} \frac{\partial^2 \tilde{c}^1}{\partial \tilde{x}^2} &= e^{\tilde{\eta}^0} (\tilde{c}^1 + \tilde{c}^0 \tilde{\eta}^1) + i \tilde{\omega} \tilde{c}^1, \quad \left. \frac{\partial \tilde{c}^1}{\partial \tilde{x}} \right|_{\tilde{x}=0} = 0, \\ \tilde{c}^1(1) &= \tilde{c}_b^1(1) \end{split} \tag{15}$$

$$\tilde{D}_{b} \frac{\partial^{2} \tilde{c}_{b}^{1}}{\partial \tilde{x}^{2}} = i \tilde{\omega} \tilde{c}_{b}^{1}, \quad \tilde{D}_{b} \frac{\partial \tilde{c}_{b}^{1}}{\partial \tilde{x}} \bigg|_{\tilde{x}=1+} = \tilde{D}_{ox} \frac{\partial \tilde{c}^{1}}{\partial \tilde{x}} \bigg|_{\tilde{x}=1-}, 
\tilde{c}_{b}^{1} (1 + \tilde{l}_{b}) = \tilde{c}_{b}^{1}$$
(16)

where  $\tilde{c}_h^I$  is the oxygen concentration perturbation at the GDLl channel interface.

From eq 16, the solution for  $\tilde{c}_b^1(\tilde{x})$  can be obtained:

$$\tilde{c}_{b}^{1}(\tilde{x}) = \frac{1}{\cosh(\tilde{l}_{b}\sqrt{i\tilde{\omega}/\tilde{D}_{b}})} \left( \cosh(\sqrt{i\tilde{\omega}/\tilde{D}_{b}})(\tilde{x}-1)) \tilde{c}_{h}^{1} + \frac{\sinh(\sqrt{i\tilde{\omega}/\tilde{D}_{b}})(\tilde{x}-1-\tilde{l}_{b}))}{\sqrt{i\tilde{\omega}\tilde{D}_{b}}} \tilde{D}_{ox} \frac{\partial \tilde{c}^{1}}{\partial \tilde{x}} \bigg|_{\tilde{x}=1-} \right)$$
(17)

Setting  $\tilde{x} = 1$  in eq 17, we find

$$\tilde{c}_b^1(1) = -\alpha \tilde{D}_{ox} \frac{\partial \tilde{c}^1}{\partial \tilde{x}} \bigg|_{\tilde{x}=1-} + \beta \tilde{c}_h^1$$
(18)

where

$$\alpha = \frac{\tanh(\tilde{l}_b \sqrt{\mathrm{i}\tilde{\omega}/\tilde{D}_b})}{\sqrt{\mathrm{i}\tilde{\omega}\tilde{D}_b}}, \quad \beta = \frac{1}{\cosh(\tilde{l}_b \sqrt{\mathrm{i}\tilde{\omega}/\tilde{D}_b})}$$
(19)

Equation 18 transforms the right boundary condition for eq 15 into the Robin-type one.

Introducing the zeta-admittance,

$$\tilde{G}(\tilde{x}) = \frac{\tilde{c}^1(\tilde{x})}{\tilde{\eta}^1}, \quad \tilde{G}_h = \frac{\tilde{c}_h^1}{\tilde{\eta}^1}$$
 (20)

and dividing eq 15 and eq 18 by  $\tilde{\eta}^1$ , we get the problem for  $\tilde{G}(\tilde{x})$ ,

$$\begin{split} \tilde{D}_{ox} \frac{\partial^2 \tilde{G}}{\partial \tilde{x}^2} &= e^{\tilde{\eta}^0} (\tilde{G} + \tilde{c}^0) + i\tilde{\omega}\tilde{G}, \quad \left. \frac{\partial \tilde{G}}{\partial \tilde{x}} \right|_{\tilde{x}=0} = 0, \\ \tilde{G}(1) &+ \alpha \tilde{D}_{ox} \frac{\partial \tilde{G}}{\partial \tilde{x}} \right|_{\tilde{x}=1-} &= \beta \tilde{G}_h \end{split}$$
(21)

where  $\tilde{G}_h$  is the measurable zeta-admittance in the channel. Substituting eq 8 into eq 21 and solving it, we find

$$\begin{split} \tilde{G}(\tilde{x}) &= \frac{\left(\mathrm{e}^{\tilde{\eta}^0} \tilde{c}_1^{\,0}(\alpha \tilde{D}_{\!ox} \phi_0^{\,} \tanh(\phi_0^{\,}) + 1\right) + \beta \tilde{G}_h^{\,} \mathrm{i}\tilde{\omega}\right) \cosh(\phi_1^{\,}\tilde{x})}{\mathrm{i}\tilde{\omega}(\alpha \tilde{D}_{\!ox} \phi_1^{\,} \sinh(\phi_1^{\,}) + \cosh(\phi_1^{\,}))} \\ &- \frac{\mathrm{e}^{\tilde{\eta}^0} \tilde{c}_1^{\,0} \cosh(\phi_0^{\,}\tilde{x})}{\mathrm{i}\tilde{\omega}^{\,} \cosh(\phi_0^{\,})} \end{split} \tag{22}$$

where

$$\phi_1 = \sqrt{\frac{e^{\tilde{\eta}^0 + i\tilde{\omega}}}{\tilde{D}_{ox}}}$$
 (23)

Differentiating eq 22 we get  $\partial \tilde{G}/\partial \tilde{x}|_{\tilde{x}=1-}$ 

$$\frac{\partial \tilde{G}(\tilde{x})}{\partial \tilde{x}} \bigg|_{\tilde{x}=1-} = \frac{\left(e^{\tilde{\eta}^0} \tilde{c}_1^0 (\alpha \tilde{D}_{ox} \phi_0 \tanh(\phi_0) + 1) + \beta \tilde{G}_h i \tilde{\omega}\right) \phi_1}{i \tilde{\omega} (\alpha \tilde{D}_{ox} \phi_1 + \coth(\phi_1))} - \frac{e^{\tilde{\eta}^0} \tilde{c}_1^0 \phi_0 \tanh(\phi_0)}{i \tilde{\omega}} \tag{24}$$

In ref 10, eq 22 has been solved for  $G_h$ , assuming that the admittance at the membrane interface is zero:  $\tilde{G}(0) = 0$ . This solution leads to a simple equation for the zeta-impedance  $\tilde{\zeta} = 1/\tilde{G}_h$  under the further assumption of large air flow stoichiometry. In the next section, we show that the assumption  $\tilde{G}(0) = 0$  can be relaxed by considering oxygen transport in the channel. This will lead us to the concept of concentration admittance at the channel outlet, as discussed below.

**Along-the-Channel Direction.** The oxygen mass transport in the channel is described by a plug flow eq 25:

$$\frac{\partial c_h}{\partial t} + \nu \frac{\partial c_h}{\partial z} = -\frac{D_b}{h} \frac{\partial c_b}{\partial x} \bigg|_{x=l_++l_h} \tag{25}$$

The right side of eq 25 is the oxygen flux at the GDLlchannel interface, describing an oxygen sink to the porous layers.

Nondimensionalization of eq 25 gives

$$\frac{\partial \tilde{c}_h}{\partial \tilde{t}} + \tilde{v} \frac{\partial \tilde{c}_h}{\partial \tilde{z}} = -\frac{\tilde{D}_b}{\tilde{h}} \frac{\partial \tilde{c}_b}{\partial \tilde{x}} \bigg|_{\tilde{x} = 1 + \tilde{l}_h}, \quad \tilde{h} = \frac{h}{l_t}$$
(26)

Linearization and Fourier-transformation of eq 26 leads to

$$\tilde{v}\frac{\partial \tilde{c}_{h}^{1}}{\partial \tilde{z}} = -i\tilde{\omega}\tilde{c}_{h}^{1} - \frac{\tilde{D}_{b}}{\tilde{h}}\frac{\partial \tilde{c}_{b}^{1}}{\partial \tilde{x}}\bigg|_{\tilde{x}=1+\tilde{l}_{b}}$$
(27)

From eq 17 we find the flux  $\partial \tilde{c}_b^1/\partial \tilde{x}|_{\tilde{x}=1+\tilde{l}_b}$ :

$$\frac{\partial \tilde{c}_b^1}{\partial \tilde{x}} \bigg|_{\tilde{x}=1+\tilde{l}_b} = i\tilde{\omega}\alpha\tilde{c}_h^1 + \beta \frac{\tilde{D}_{ox}}{\tilde{D}_b} \frac{\partial \tilde{c}^1}{\partial \tilde{x}} \bigg|_{\tilde{x}=1-}$$
(28)

Dividing eq 27 and eq 28 by  $\tilde{\eta}^1$ , we find

$$(\tilde{h} + \alpha \tilde{D}_b) i\tilde{\omega} \tilde{G}_h + \tilde{v} \tilde{h} \frac{\partial \tilde{G}_h}{\partial \tilde{z}} = -\beta \tilde{D}_{ox} \frac{\partial \tilde{G}}{\partial \tilde{x}} \bigg|_{\tilde{v}=1-}$$
(29)

Substituting eq 24 into eq 29 and using the identity  $\lambda \tilde{J} = \tilde{\nu} \tilde{h}$ , we arrive at

$$\frac{\partial \tilde{G}_h}{\partial \tilde{z}} + P\tilde{G}_h = Q\tilde{c}_1^0, \quad \tilde{G}_h(0) = \tilde{G}_{h,0}$$
(30)

where  $\tilde{J}$  is described through the equation of the polarization curve at finite stoichiometry  $^{12}$ 

$$-\lambda \ln \left(1 - \frac{1}{\lambda}\right) \tilde{J} = e^{\tilde{\eta}^0} \tag{31}$$

and

$$P = \frac{1}{\lambda \tilde{J}} \left[ i\tilde{\omega}(\tilde{h} + \alpha \tilde{D}_b) + \frac{\beta^2 \tilde{D}_{ox} \phi_1}{\alpha \tilde{D}_{ox} \phi_1 + \coth(\phi_1)} \right]$$
(32)

$$Q = -\frac{\beta \tilde{D}_{ox} e^{\tilde{\eta}^0} \tanh(\phi_0)}{i\tilde{\omega}\lambda \tilde{J}} \left( \frac{\alpha \tilde{D}_{ox} \phi_0 + \coth(\phi_0)}{\alpha \tilde{D}_{ox} \phi_1 + \coth(\phi_1)} \phi_1 - \phi_0 \right)$$
(33)

Note that the boundary condition for eq 30 stems from the perturbation of oxygen concentration applied at the channel inlet (see below).

Substituting eq 14 into eq 30, we obtain the solution for  $G_h$ 

$$\tilde{G}_{h}(\tilde{z}) = \tilde{G}_{h,0} \exp(-P\tilde{z}) + \frac{Q_{1}}{P + \ln(1 - 1/\lambda)} \left( \left(1 - \frac{1}{\lambda}\right)^{\tilde{z}} - \exp(-P\tilde{z}) \right)$$
(34)

where

$$Q_{1} = \frac{Q}{1 + \tilde{D}_{0x}\phi_{0} \tanh(\phi_{0})\tilde{l}_{b}/\tilde{D}_{b}}$$
(35)

In the following, we will be interested in the admittance at the channel outlet assuming zero perturbation of the oxygen concentration at the inlet. Setting  $\tilde{G}_{h,0}=0$  and  $\tilde{z}=1$  in eq 34, we finally find

$$\tilde{G}_{h,1} = \frac{Q_1(1 - 1/\lambda - \exp(-P))}{P + \ln(1 - 1/\lambda)}$$
(36)

#### ■ RESULTS AND DISCUSSION

**Parameterization and Simulation.** The Nyquist spectrum of eq 36 consists of a large loop in the frequency range from 0.1 to 2 Hz and multiple small loops above 2 Hz (Figure 2). The small loops arise due to the interference of local

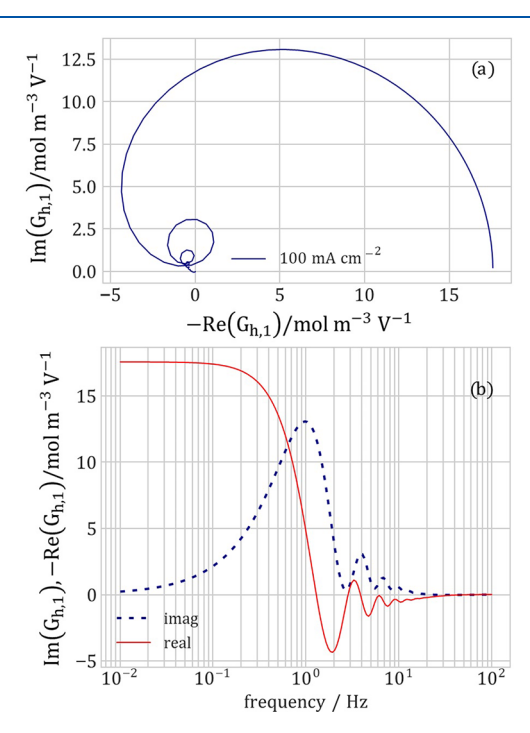


**Figure 2.** (a) Nyquist spectrum of eq 36 for the parameters in Table 1. (b) Frequency dependence of the real and imaginary parts of the spectrum in part a.

perturbations of the oxygen concentration with perturbations transported along the channel. Similar loops have been reported in local EIS spectra. The nature of the small loops will be analyzed in detail in a follow-up publication. The parameters to calculate the spectra shown in Figure 2 are listed in Table 1. The static value of  $G_{h,1}^0$  (at zero frequency) depends on the oxygen transport parameters in the GDL and CCL.

#### Table 1. Cell Parameters Used in Calculations

Tafel slope b, V	0.03
exchange current density i*, A cm <sup>-3</sup>	$10^{-3}$
oxygen diffusion coefficient in the CCL, $^{15}$ $D_{ox}$ , cm <sup>2</sup> s <sup>-1</sup>	$10^{-4}$
oxygen diffusion coefficient in the GDL, $^{15}$ $D_b$ , cm $^2$ s $^{-1}$	$2 \times 10^{-2}$
catalyst layer thickness $l_v$ cm	$10 \times 10^{-4}$
gas diffusion layer thickness $l_b$ , cm	$200 \times 10^{-4}$
channel height h, cm	0.1
cell current density J, A cm <sup>-2</sup>	0.1
pressure	standard
cell temperature T, K	273 + 80
air flow stoichiometry, $\lambda$	10

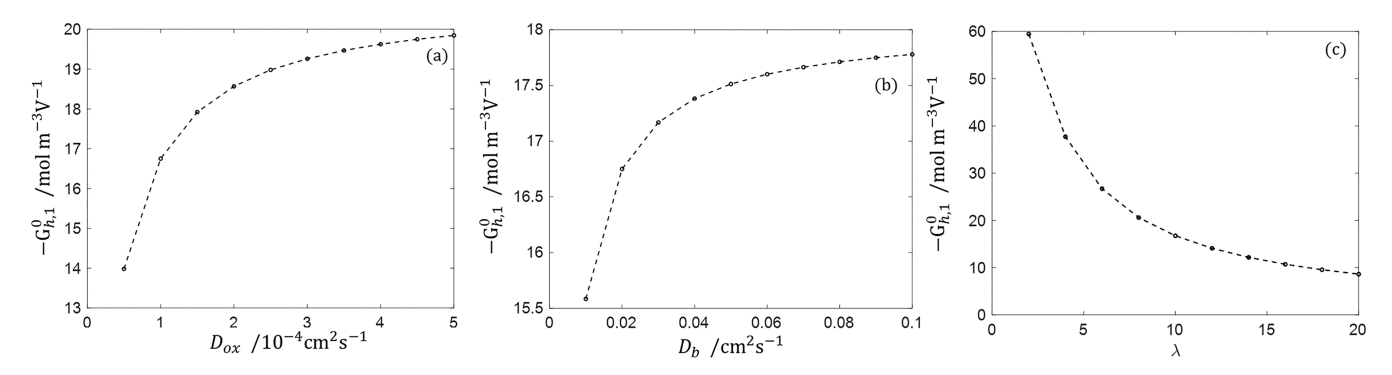


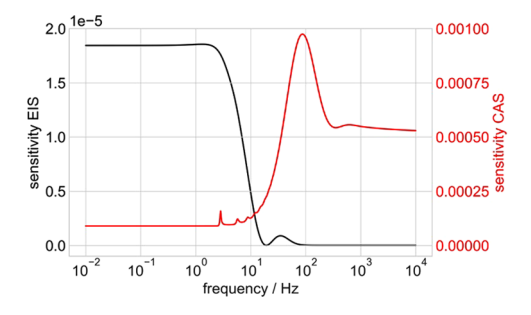
Figure 3. Static zeta-admittance  $G_{h,1}^0$  vs (a) the oxygen diffusion coefficient in the CCL  $D_{ox}$ . (b) Oxygen diffusion coefficient in the GDL  $D_b$ . (c) Stoichiometry of air flow  $\lambda$ .

Here, we show the dependence of  $\tilde{G}_{h,1}^0$  on the stoichiometry of air flow  $\lambda$ , the oxygen diffusion coefficient in the GDL  $D_{bv}$  and the oxygen diffusion coefficient in the CCL  $D_{ox}$ . As shown in parts a and b of Figure 3, the higher  $D_{ox}$  and  $D_{bv}$ , the larger  $\tilde{G}_{h,1}^0$  is. Figure 3c illustrates that with increase of  $\lambda$ ,  $\tilde{G}_{h,1}^0$  decreases. Indeed, the larger the stoichiometry, the smaller is the oxygen concentration variation along the channel and therefore the lower is the static zeta-admittance.

A sensitivity analysis of simulated concentration admittance spectra (CAS) in comparison with EIS in terms of oxygen diffusion coefficient in the CCL  $D_{ox}$  is performed. Here, we define the relative sensitivity  $S_R$  as:

$$S_{R} = \frac{\delta |Y|/|Y|}{\delta D_{ox}/D_{ox}} \tag{37}$$

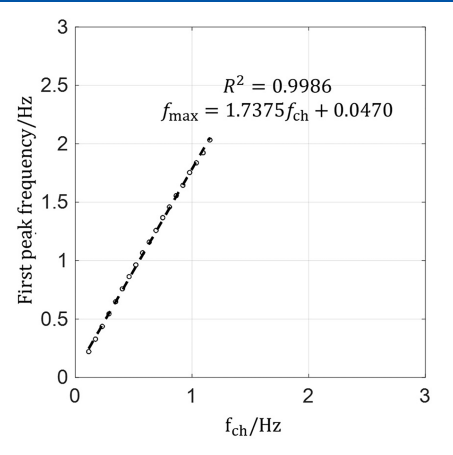
where  $\delta D_{ox}$  is the absolute value of the oxygen diffusion coefficient variation, |Y| is the magnitude of the corresponding electrochemical impedance or concentration admittance, respectively, at the initial value of  $D_{ox}$ , and  $\delta |Y|$  is the change in magnitude of electrochemical impedance or concentration admittance (i.e.,  $\delta |Y| = |Y_{D_{ox}} + \delta D_{ox}| - |Y_{D_{ox}}|$ ). The advantage of this definition is that it allows for a comparison between different methods, which would have values in different units and orders of magnitude. In addition,  $S_R$  characterizes solely the model, excluding any influence of measurement inaccuracy. The sensitivity analysis of simulated CAS in comparison with conventional EIS for the oxygen diffusion coefficient in the CCL  $D_{ox}$  is shown in Figure 4, where  $\delta D_{ox}/D_{ox} = 0.05$ . Figure 4 illustrates that the CAS has a higher sensitivity over the frequency range of 0.01 Hz to 10<sup>4</sup> Hz compared to EIS. The highest sensitivity of CAS is around 100 Hz, while that of EIS is at frequencies below 1 Hz.



**Figure 4.** Sensivity of oxygen diffusion coefficient in the CCL  $D_{ox}$  of EIS and concentration admittance spectroscopy (CAS).

Note that this increase of *relative* sensitivity at high frequency comes with a decrease in *absolute* magnitude of the concentration admittance. The latter will lead to a lower sensitivity of the measurement equipment, counterbalancing the increasing sensitivity of the model. To pinpoint the best frequency for measuring the oxygen diffusion coefficient by means of CAS, a combined consideration of the equipment's limitation and the relative sensitivity analysis is needed. However, while the sensitivity of EIS approaches zero, the sensitivity of CAS has finite and generally larger values ( $\approx 1$  order of magnitude) for all frequencies.

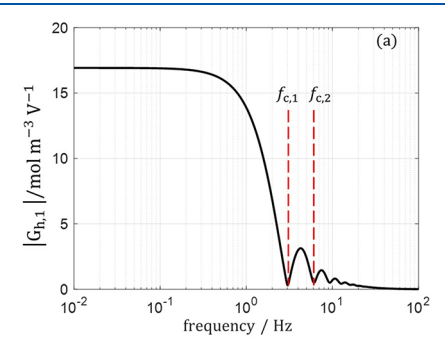
A parametric study is performed to determine the relationship between the position  $f_{max}$  of the leftmost peak of the zeta-admittance's imaginary part Im  $(G_{h,1})$  and the stoichiometry of air flow  $\lambda$  with the corresponding characteristic frequency of the channel,  $f_{ch} = v/(2\pi L)$ . The simulation of CAS is carried out with the parameters from Table 1 and by varying the stoichiometry of air flow  $\lambda$  from 2 to 20. The frequency of the leftmost peak  $f_{max}$  is plotted against  $f_{ch}$  in Figure 5. The



**Figure 5.** Position  $f_{max}$  of the first (leftmost) peak of imaginary part of zeta-admittance  $G_{h,1}$  in Figure 2 vs the characteristic frequency of the channel  $f_{ch} = \nu/(2\pi L)$ .

position of  $f_{max}$  is proportional to the stoichiometry of air flow  $\lambda$  and to the corresponding  $f_{ch}$ . As shown in Figure 5,  $f_{max}$  can be used to extract the characteristic frequency of the oxygen transport in channel. Note that this particular linear dependence is only valid for the channel depth h of 0.1 cm. For other values of h, the slope of linear dependence will vary. The slopes for channel depth of 0.05, 0.1, and 0.2 cm are 1.35, 1.74, and 2.00, respectively.

The magnitude and phase Bode plots of eq 36 are shown in Figure 6. As seen, the magnitude of  $G_{h,1}$  decreases with the



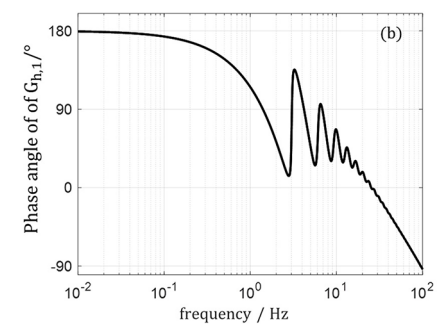


**Figure 6.** (a) Magnitude Bode plot of eq 36 for the parameters in Table 1. (b) Phase Bode plot of eq 36 for the parameters in Table 1.

increase of frequency and reaches a minimum value at a critical frequency  $f_{c,1} = 3.0$  Hz. The magnitude then exhibits periodic oscillations upon further increasing the frequency. It reaches another local minima at the frequencies, which are multiples of the critical frequency, e.g.,  $f_{c,2} = 6.0$  Hz, which is twice  $f_{c,1}$ . The time constant corresponding to the critical frequency  $t_{c,1} = 1/f_{c,1} = 0.33$  s is close to the time for oxygen travel from inlet to outlet  $t_{ch} = L/v = 0.28$  s. This trend could be attributed to the interference of local perturbations of oxygen concentration with perturbations transported along the channel. A detailed study of this effect will be performed in future work. A similar effect has been reported by Sorrentino.

**Suggested Experimental Setup.** Equation 36 can be used for fitting of experimental spectra of the cell admittance, provided that the spectrum of oxygen concentration oscillations can be measured at the channel outlet. Note that the experimental procedure does not require excitation of the outlet air pressure. The principal method is the same as for standard EIS measurements. However, in addition to measuring the electric variables, the spectrum  $G_{h,1}^1$  at the channel outlet has to be measured.

An oxygen sensor could be used to measure the oxygen concentration at the cathode outlet if the sensor meets the precision and frequency requirements of concentration admittance spectroscopy. Alternatively, the measurement could be done by supplying the outlet air flow to the cathode of a separate measurement cell with minimal oxygen transport losses and well-characterized electric properties. This could be a button-type cell with a catalyst coated membrane operating at a small current density. The schematic of this experimental setup is shown in Figure 7. The incoming oscillations of the oxygen concentration would produce oscillations of the

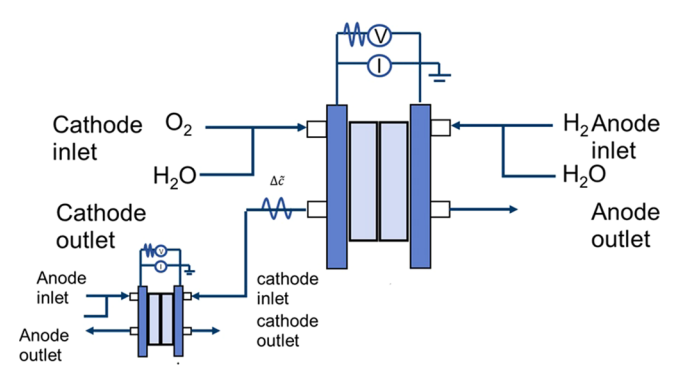


**Figure 7.** Schematic of the proposed experimental setup for the measurement of the concentration variation at the cathode outlet of PEFC.

voltage,  $E_m^1$ , of this measurement cell, referred to as the *m*-cell. In the absence of oxygen transport losses,  $E_m^1$  allows one to calculate the required spectrum of  $c_{h,1}^1(\omega)$ :

$$c_{h,1}^{1} = \frac{-E_{m}^{1}c_{m}^{0} \exp(E_{m}^{0}/b_{m})}{l_{t,m}i_{*,m}} \left(\frac{1}{Z_{m}} - iC_{dl,m}l_{t,m}\omega\right) + \frac{c_{m}^{0}E_{m}^{1}}{b_{m}}$$
(38)

Here  $Z_m$  is the electrochemical impedance and all the other parameters on the right side refer to the m-cell, as indicated. Equation 38 follows from the proton charge conservation equation in the m-cell catalyst layer. Dividing  $c_{h,1}^1$  by  $E^1$  of the test cell,  $G_{h,1}$  can be obtained.

There are several advantages of CAS over *C/P* impedance spectroscopy. First, CAS can be measured simultaneously with the standard EIS. Hereby, the sensitivity of both methods can complement each other, enhancing the accuracy of the extracted parameters. Second, there is no need to apply any concentration or pressure perturbation at the cathode inlet/outlet. Last but not least, CAS does not require keeping zero total current perturbation in the system.

### CONCLUSIONS

A model for the concentration admittance  $G_{h,1}$  at the cathode channel outlet of a PEFC has been presented. The model is based on oxygen mass transport equations in the flow field channel, gas diffusion layer, and catalyst layer. An analytical expression for  $G_{h,1}$  has been derived assuming that the perturbation of the oxygen concentration at the channel inlet remains zero. The solution suggests a novel method for PEFC characterization: in a standard EIS experiment, measuring oscillations in the outlet oxygen concentration  $\delta c_{h,1}$  allows one to calculate  $G_{h,1} = \delta c_{h,1}/\delta \eta$ . The analytical solution for  $G_{h,1}$ could be fitted to experimental spectra, giving an independent means for the determination of oxygen transport parameters in the cell. The measurement of  $\delta c_{h,1}$  could be conducted by supplying the air flow from the channel outlet of the cell being probed to a separate measurement cell, which could be a button fuel cell with minimal oxygen transport losses. The EIS spectrum of this cell can be directly related to the concentration admittance  $G_{h,1}$ . Overall, concentration admittance spectroscopy can be measured simultaneously to standard EIS using easy instrumentation, greatly enhancing the sensitivity and the accuracy of extracted transport parameters.

#### AUTHOR INFORMATION

#### **Corresponding Authors**

Ying Sun - Theory and Computation of Energy Materials (IEK-13), Institute of Energy and Climate Research, Forschungszentrum Jülich GmbH, D-52425 Jülich, Germany; Chair of Theory and Computation of Energy Materials, Faculty of Georecources and Materials Engineering, RWTH Aachen University, D-52062 Aachen, Germany; Email: y.sun@fz-juelich.de

Andrei Kulikovsky - Theory and Computation of Energy Materials (IEK-13), Institute of Energy and Climate Research, Forschungszentrum Jülich GmbH, D-52425 Jülich, Germany; orcid.org/0000-0003-1319-576X; Email: a.kulikovsky@fz-juelich.de

#### **Authors**

Thomas Kadyk – Theory and Computation of Energy Materials (IEK-13), Institute of Energy and Climate Research, Forschungszentrum Jülich GmbH, D-52425 Jülich, Germany; JARA Energy, Jülich Aachen Research Alliance, D-52425 Jülich, Germany

Michael Eikerling - Theory and Computation of Energy Materials (IEK-13), Institute of Energy and Climate Research, Forschungszentrum Jülich GmbH, D-52425 Jülich, Germany; Chair of Theory and Computation of Energy Materials, Faculty of Georecources and Materials Engineering, RWTH Aachen University, D-52062 Aachen, Germany; JARA Energy, Jülich Aachen Research Alliance, D-52425 Jülich, Germany; orcid.org/0000-0002-0764-

Complete contact information is available at: https://pubs.acs.org/10.1021/acs.jpcc.2c04131

#### **Notes**

The authors declare no competing financial interest.

#### ACKNOWLEDGMENTS

The authors thank Forschungszentrum Jülich for support during this work.

# REFERENCES

- (1) Niroumand, A. M.; Mérida, W.; Eikerling, M.; Saif, M. Pressurevoltage oscillations as a diagnostic tool for PEFC cathodes. Electrochem. Commun. 2010, 12, 122-124.
- (2) Engebretsen, E.; Mason, T. J.; Shearing, P. R.; Hinds, G.; Brett, D. J. Electrochemical pressure impedance spectroscopy applied to the study of polymer electrolyte fuel cells. Electrochem. Commun. 2017,
- (3) Zhang, Q.; Eikerling, M. H.; Gates, B. D. Electrochemical pressure impedance spectroscopy as a diagnostic method for hydrogen-air polymer electrolyte fuel cells. ECS Meeting Abstracts 2020, MA2020-02, 1586.
- (4) Zhang, Q.; Homayouni, H.; Gates, B.; Eikerling, M.; Niroumand, A. Electrochemical Pressure Impedance Spectroscopy for Polymer Electrolyte Fuel Cells via Back-Pressure Control. J. Electrochem. Soc. 2022, 169, 044510.
- (5) Shirsath, A. V.; Raël, S.; Bonnet, C.; Lapicque, F. Electrochemical pressure impedance spectroscopy applied to polymer electrolyte membrane fuel cells for investigation of transport phenomena. Electrochim. Acta 2020, 363, 137157.
- (6) Schiffer, L.; Shirsath, A. V.; Raël, S.; Bonnet, C.; Lapicque, F.; Bessler, W. G. Electrochemical Pressure Impedance Spectroscopy for Polymer Electrolyte Membrane Fuel Cells: A Combined Modeling and Experimental Analysis. J. Electrochem. Soc. 2022, 169, 034503.

- (7) Sorrentino, A.; Vidakovic-Koch, T.; Hanke-Rauschenbach, R.; Sundmacher, K. Concentration-alternating frequency response: A new method for studying polymer electrolyte membrane fuel cell dynamics. Electrochim. Acta 2017, 243, 53-64.
- (8) Sorrentino, A.; Vidakovic-Koch, T.; Sundmacher, K. Studying mass transport dynamics in polymer electrolyte membrane fuel cells using concentration-alternating frequency response analysis. J. Power Sources 2019, 412, 331-335.
- (9) Sorrentino, A.; Sundmacher, K.; Vidakovic-Koch, T. Decoupling oxygen and water transport dynamics in polymer electrolyte membrane fuel cells through frequency response methods based on partial pressure perturbations. Electrochim. Acta 2021, 390, 138788.
- (10) Kulikovsky, A. Analytical model for PEM fuel cell concentration impedance. J. Electroanal. Chem. 2021, 899, 115672.
- (11) Kubannek, F.; Krewer, U. Studying the interaction of mass transport and electrochemical reaction kinetics by species frequency response analysis. J. Electrochem. Soc. 2020, 167, 144510.
- (12) Kulikovsky, A. A. The Effect of Stoichiometric Ratio  $\lambda$  on the Performance of a Polymer Electrolyte Fuel Cell. Electrochim. Acta 2004, 49, 617-625.
- (13) Kulikovsky, A. Analytical physics-based impedance of the cathode catalyst layer in a PEM fuel cell at typical working currents. Electrochim. Acta 2017, 225, 559-565.
- (14) Kulikovsky, A. A. A Model for Local Impedance of the Cathode Side of PEM Fuel Cell With Segmented Electrodes. J. Electrochem. Soc. 2012, 159, F294-F300.
- (15) Reshetenko, T.; Kulikovsky, A. Variation of PEM fuel cell physical parameters with current: Impedance spectroscopy study. J. Electrochem. Soc. 2016, 163, F1100.
- (16) Sorrentino, A. Frequency response analysis based on concentration inputs for the study and diagnosis of polymer electrolyte membrane fuel cells. Ph.D. Thesis; Fakultät für Verfahrensund Systemtechnik, Otto-von-Guericke-Universität Magdeburg: 2021.

# **□** Recommended by ACS

Investigation of Water Oxidation at IrO2 Electrodes in Nafion-Based Membrane Electrode Assemblies Using Impedance Spectroscopy and Distribution of Relaxation...

Patrick K. Giesbrecht and Michael S. Freund

OCTOBER 16, 2022

THE JOURNAL OF PHYSICAL CHEMISTRY C

**Experimental Study of Electronic and Ionic Conductivity of** a Carbon-Based Slurry Electrode Used in Advanced **Electrochemical Energy Systems** 

Monjur Mourshed, Bahman Shabani, et al.

AUGUST 24 2022

ACS APPLIED ENERGY MATERIALS

READ **C** 

# Streaming Potential with Ideally Polarizable Electron-**Conducting Substrates**

Andriy Yaroshchuk and Emiliy Zholkovskiy

AUGUST 04, 2022

LANGMUIR

READ **C** 

Correlation between the Forming Sites of Hydrogen Bubbles and Micro/Nanostructures on the Electrode Surface

Kota Ando, Takashi Nakajima, et al.

OCTOBER 26, 2022

THE JOURNAL OF PHYSICAL CHEMISTRY C

RFAD 🗹

Get More Suggestions >